

Discy dwarf disruption and the shape of the Galactic halo

S.L.J. Gibbons^{1*}, V. Belokurov¹, D. Erkal¹ and N.W. Evans¹

¹*Institute of Astronomy, University of Cambridge, Madingley Road, Cambridge, CB3 0HA, UK*

Accepted 2016 January 27. Received 2016 January 7; in original form 2015 November 4

Accepted version. This is a pre-copyedited, author-produced version of an article accepted for publication in MNRAS following peer review.

ABSTRACT

The shape of the Galactic dark halo can, in principle, be inferred through modelling of stellar tidal streams in the Milky Way halo. The brightest and the longest of these, the Sagittarius stream, reaches out to large Galactocentric distances and hence can deliver the tightest constraints on the Galaxy’s potential. In this contribution, we revisit the idea that the Sagittarius Stream was formed from a rotating progenitor. We demonstrate that the angle between the disk’s angular momentum and the progenitor’s orbital angular momentum does not remain constant throughout the disruption. Instead, it undergoes a dramatic evolution caused, in part, by the changes in the progenitor’s moment of inertia tensor. We show that, even in a spherical potential, the streams produced as a result of a discy dwarf disruption appear to be “precessing”. Yet, this debris plane evolution is illusory as it is solely caused by the swaying and wobbling of the progenitor’s disk. Stream plane precession is therefore not an unambiguous indicator of asphericity of the dark halo.

Key words: Galaxy: halo – Galaxy: kinematics and dynamics – galaxies: dwarf: Sagittarius

1 INTRODUCTION

The shape and the orientation (if it is aspherical) of the dark halo of the Milky Way encodes information as to the assembly of the Galaxy, i.e. its accretion history (e.g. Allgood et al. 2006); the interplay between Dark Matter (DM) and baryons (see e.g. Kazantzidis et al. 2004; Debattista et al. 2008; Abadi et al. 2010); the nature of the DM particle (e.g. Dubinski & Carlberg 1991; Davé et al. 2001; Mayer et al. 2002); and even the Cosmology itself (e.g. Macciò et al. 2008). Complicating the picture is the fact that the DM halo shape is likely to vary with Galactocentric radius (e.g. Hayashi et al. 2007; Vera-Ciro et al. 2011). Unfortunately, only a handful of techniques currently exist to gauge the Galactic DM halo shape (e.g. Gnedin et al. 2005; Yu & Madau 2007; Smith et al. 2009; Loebman et al. 2012). Of the few methods available, inference based on the stellar streams dynamics appears to be one of the most promising methods (see e.g. Helmi 2004; Law et al. 2005; Koposov et al. 2010). To probe regions of the Milky Way dominated by the DM halo, streams reaching to large Galactocentric radii are required. Covering distances between 15 and 100 kpc, the Sagittarius (Sgr) stream offers exceptional leverage. However, all attempts to interpret the Sgr stream data thus far have led to conflicting claims as to the shape of the Galactic halo (Helmi 2004; Johnston et al. 2005; Fellhauer et al. 2006; Law & Majewski 2010).

The asphericity of the halo produces a non-radial component of the gravitational force, and the ensuing torques cause the debris plane to precess. The evolution of the Sgr stream plane has

been measured with high accuracy (Belokurov et al. 2014), but the picture is confused by the presence of two distinct branches, separated by $\sim 10^\circ$, for both the leading and the trailing tail (Belokurov et al. 2006; Koposov et al. 2012). Moreover, as shown by Belokurov et al. (2014), the two branches in the bifurcation appear to precess by different amounts and in different directions. To advance our understanding of the Galactic gravitational potential, a reliable model of the Sgr disruption needs to be found that would explain the entirety of the Sgr data, including the enigmatic stream bifurcation. Peñarrubia et al. (2010) have shown that a rotating progenitor (i.e. a disk galaxy) provides a natural explanation of such stream forking. In their picture, the velocities of unbound stars are a combination of the progenitor’s systemic velocity and the disk rotation velocity at the moment of stripping. If the disk and the orbital plane are misaligned, the two velocity vectors change orientation with respect to each other as the dwarf orbits the Galaxy. Therefore, in every stripping episode, the debris are sprayed at a different angle with respect to the orbital plane (see also Amorisco 2015). The angular separation between individual streamlets is controlled by two parameters: i) the angle between the progenitor’s disk and orbital plane; and ii) the rotational velocity of the progenitor.

Peñarrubia et al. (2010) predicted that, if their realisation of the Sgr disruption were correct, a residual rotational signal of $\sim 20 \text{ kms}^{-1}$ ought to be present in the remnant. However, a number of studies have found only a very modest level of rotation in the Sgr core, typically $< 4 \text{ kms}^{-1}$ (e.g., Peñarrubia et al. 2011; Frinchaboy et al. 2012). This remains a serious obstacle for scenarios in which the Sgr progenitor is a rotating disk dwarf. Even so, the still poorly understood transformation of rotating dwarf irregulars

* E-mail: sljg2@ast.cam.ac.uk

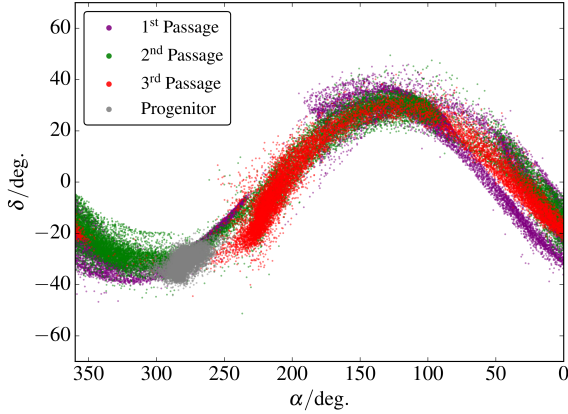


Figure 1. Distribution of the stream particles of the leading arm on the sky. The particles are color-coded according to the pericentre passage at which they are released. In this simulation, the disk’s angular momentum vector is initially misaligned by 40° with the orbital angular momentum vector. Note that the stream appearance is different from the usual case of a dSph disruption: the streamlets corresponding to different pericentre crossing times are sprayed in slightly different directions.

to non-rotating dwarf spheroidals shows that mechanisms do exist to shed angular momentum. Alternately, stellar rotation may dominate in the outer parts of the progenitor, but the inner parts may be supported by velocity dispersion (e.g., the case of WLM in Leaman et al. 2012), leaving a remnant with little or no residual rotation after stripping. Whilst acknowledging the seriousness of this problem, we do believe it is premature to rule out the entire class of stream models based on rotating progenitors without a thorough exploration of parameter space. Motivated by the development of a new generation of fast and accurate tidal stream models are becoming available (see Gibbons et al. 2014; Bowden et al. 2015; Küpper et al. 2015; Amorisco et al. 2015), we examine a representative simulation of a disk dwarf disruption, in order to build insight into this largely unexplored regime of stellar stream formation.

2 DISKY DWARF DISRUPTION

To set up the initial conditions of the progenitor we use the MAGALIE code from the NEMO stellar dynamics toolbox. This employs the algorithm presented in Boily et al. (2001) to construct realisations of composite progenitors comprised of stellar disks embedded within DM haloes. In choosing the structural parameters for the progenitor we followed Peñarrubia et al. (2010). More precisely, for the stellar disk we used an exponential density profile:

$$\rho_{\text{disk}} = \frac{M_d}{4\pi R_d^2 z_d} \exp(-R/R_d) \text{sech}^2(z/z_d), \quad (1)$$

where M_d is the mass, R_d is the radial scale length of the disk and z_d is the vertical scale height. We chose to fix these at $M_d = 3.5 \times 10^8 M_\odot$, $R_d = 0.9 \text{ kpc}$. Additionally, we assumed that the vertical scale height is related to the radial scale length by $z_d = 0.2 R_d$. For the progenitor’s DM halo, we used the density profile:

$$\rho_{\text{halo}} = \frac{M_h \alpha(r_c/r_{\text{cut}}) \exp(-r^2/r_{\text{cut}}^2)}{2\pi^{3/2} r_{\text{cut}} (r^2 + r_c^2)}, \quad (2)$$

where $M_h = 2.4 \times 10^9 M_\odot$ is the halo mass, $r_c = 0.5 R_d$ is the core radius and $r_{\text{cut}} = 6 R_d$ is the radius at which the halo is truncated. For these values of the structural parameters $\alpha \approx 1.156$.

We imposed the truncation to the halo as the outer envelope of the progenitor’s dark halo is likely to be lost before the stream begins to form. This is in line with the results reported by Niederste-Ostholt et al. (2010) who found that the outer parts of the halo are lost before the majority of stellar particles are stripped. The dwarf’s circular velocity curve is therefore a combination of the contributions from the disk and the halo, and peaks at 47 km s^{-1} at 2.7 kpc .

We evolved the progenitor in a fixed spherical NFW model (Navarro et al. 1996) with $M_{200} = 7.5 \times 10^{11} M_\odot$ and concentration $c_{200} = 20$. This is not meant to be a realistic model of the Galactic potential but is just a simple representation, convenient in isolating the effects of rotation in the progenitor on the stream particles, aside from any asphericity in the host potential. The satellite is placed on an orbit with an apocentre of $r_a = 70 \text{ kpc}$, a pericentre of $r_p = 18 \text{ kpc}$, and an orbital period of $\approx 1.2 \text{ Gyr}$. The simulations were carried out using the NBODY solver in GADGET-2 (Springel 2005) which was modified to implement a static NFW potential by adding an additional force component, dependent on position, at each force computation.

Figure 1 displays the on-sky distribution of particles of the leading arm for a satellite disruption simulation where the dwarf’s disk is initially misaligned with its orbital plane by 40° . The stream particles are coloured according to the epoch during which they became unbound from the progenitor: the first to go were the particles shown in purple (1st pericentric passage); followed by the green; and finally the most recently stripped particles are shown in red. If the stream’s progenitor were not rotating or if the disk and the orbital plane were aligned, given that the host’s potential is spherical the debris stripped at different epochs would keep piling up on top of one another. However, as shown in the Figure, the situation is markedly different for the misaligned disruption, as already found by Peñarrubia et al. (2010). Here, streamlets corresponding to individual stripping episodes are clearly offset on the sky, implying that they stay in distinct orbital planes.

3 APPARENT STREAM PRECESSION AND DISK WOBBLING

Streamlet precession. Let us have a closer look at the plane evolution of the debris stripped during each pericentre crossing. The left panel of Figure 2 gives the “unwrapped” view of the stream in the plane of Galactocentric distance and angle along the stream Λ . In these coordinates, it is straightforward to isolate the debris belonging to each stripping episode. Having thus separated the particles into three groups, we can measure their orbital plane evolution. More precisely, for each bin in Λ (the boundaries of the three bins used in this analysis are shown with black vertical lines in the left panel of the Figure), the plane of the debris is assumed to be constant, well-described by its normal vector $\hat{\mathbf{n}}$, with the particles scattered about this plane by a Gaussian with variance Δ . We chose to parameterize the normal vector in terms of Galactocentric coordinates defined as $\hat{\mathbf{n}} = \cos b_p \cos l_p \hat{\mathbf{x}} + \cos b_p \sin l_p \hat{\mathbf{y}} + \sin b_p \hat{\mathbf{z}}$.

With these assumptions, the likelihood of the given normal and the variance is thus:

$$\log \mathcal{L} = - \sum_{i=1}^N \frac{(\hat{\mathbf{n}} \cdot \mathbf{x}_i)^2}{2\Delta} - \frac{N}{2} \log \Delta, \quad (3)$$

where N is the number of particles in the bin, the \mathbf{x}_i ’s are the 3D positions of each of the particles and the sum is taken over all of the particles in the bin.

Debris plane evolution for each of the three stripping epochs

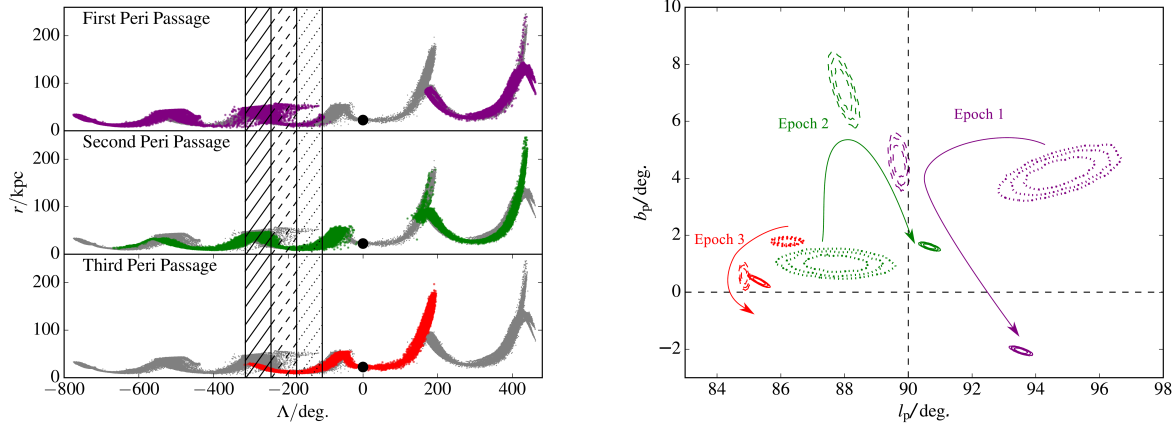


Figure 2. *Left:* Simulated stream in “unwrapped” coordinates: the particles’ Galactocentric distance is shown as a function of the angle along the stream Λ . Poles for the debris planes are extracted for three Λ bins along the leading arm (marked by black vertical lines) for each of the three stripping epochs. The current position of the progenitor is marked with a black dot. *Right:* Locations of the poles extracted in the Galactocentric coordinates. The dotted, dashed and solid contours respectively correspond to the bins marked on the left panel, moving away from the progenitor. The colours correspond to the three stripping epochs, as defined in the left hand panel. The intersection of the black dashed lines indicate the pole of the progenitor’s orbit. Arrows give the direction of the precession away from the progenitor’s location. Note that in the overlapping regions of the sky, the debris stripped at different pericentre passages precess with different amplitudes and in different directions.

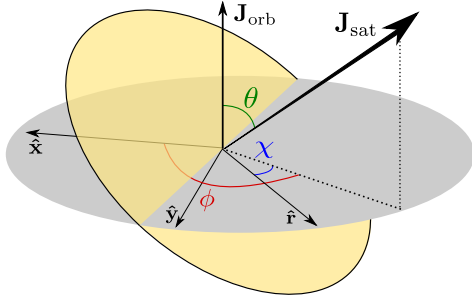


Figure 3. A schematic diagram showing the orientation angles of the disk. θ is the angle between \mathbf{J}_{orb} and \mathbf{J}_{sat} . ϕ and χ are the angles between the projection of \mathbf{J}_{sat} into the plane of the orbit and the Galactocentric \hat{x} and \hat{r} vectors respectively.

is presented in the right panel of Figure 2. It is clear that as one steps along the leading arm of the stream, away from the progenitor (as indicated by varying contour styles and the arrows), swarms of particles from each of the three pericentric passages show qualitatively dissimilar behavior, with the plane of each individual spray of debris precessing with a different amplitude and direction. This behavior is qualitatively similar to that observed in Figure 13 of Belokurov et al. (2014) where the bright arm of the bifurcation (Branch A) appears to be precessing with a much smaller amplitude, and in the opposite direction to, the faint arm of the stream (Branch B). These results therefore suggest that the bright arm of the bifurcation could have been formed from the debris that is (dynamically) younger than the faint arm. Curiously, this conflicts with the simulation presented by Peñarrubia et al. (2010). We note, however, that our interpretation is in agreement with the recent measurement of the chemical abundance differences between the two branches by Koposov et al. (2012). They report that Branch B appears to lack the metal-rich populations that are discernible in Branch A, therefore implying that this debris could have been stripped earlier.

Disk wobble and precession. The strong apparent precession

of the streamlets that is visible in the right panel of Figure 2 is surprising as the simulation of the discy dwarf disruption was performed in a spherical potential, where there are no torques acting on the stripped particles. However, there are torques acting on the progenitor’s disk, making it wobble and precess as it disrupts. The torque acting on a disk, with a density distribution $\rho(\mathbf{r})$, located in an external potential Φ , and with its centre of mass at a position \mathbf{r}_0 is:

$$\frac{d\mathbf{J}_{\text{sat}}}{dt} = - \int d^3\mathbf{r} \rho(\mathbf{r}) \mathbf{r} \times \nabla\Phi(\mathbf{r}_0 + \mathbf{r}). \quad (4)$$

If we assume that the force on the disk is slowly varying with position, we can expand the gradient of the potential about the center of mass of the progenitor to obtain:

$$\nabla\Phi(\mathbf{r}_0 + \mathbf{r})|_i \approx \nabla\Phi(\mathbf{r}_0)|_i + \sum_{k=1}^3 H_{ki}x_k + \mathcal{O}(x^2). \quad (5)$$

Here $H_{ij} \equiv \partial_i\partial_j\Phi$ is the Hessian of the potential evaluated at the centre of mass of the progenitor. In a frame centered on the disk with basis vectors \mathbf{e}_1 , \mathbf{e}_2 and \mathbf{e}_3 aligned with the symmetry axes of the disk, the torque is

$$\frac{d\mathbf{J}_{\text{sat}}}{dt} \approx H_{23}(I_3 - I_2)\mathbf{e}_1 + H_{13}(I_1 - I_3)\mathbf{e}_2 + H_{12}(I_2 - I_1)\mathbf{e}_3, \quad (6)$$

where the I_i are the principal axes of the moment of inertia tensor of the disk, defined as $I_i = \int d^3\mathbf{r} \rho(\mathbf{r})x_i^2$. For an exponential disk, these can be evaluated as:

$$I_1 = I_2 = 3M_d R_d^2; \quad I_3 = \frac{1}{12}M_d \pi^2 z_d^2 \quad (7)$$

We followed changes in the disk’s orientation during its orbit around the Milky Way, as described by the following three angles (see Figure 3): θ is the angle between the orbital angular momentum, \mathbf{J}_{orb} , and the satellite’s internal angular momentum, \mathbf{J}_{sat} ; ϕ

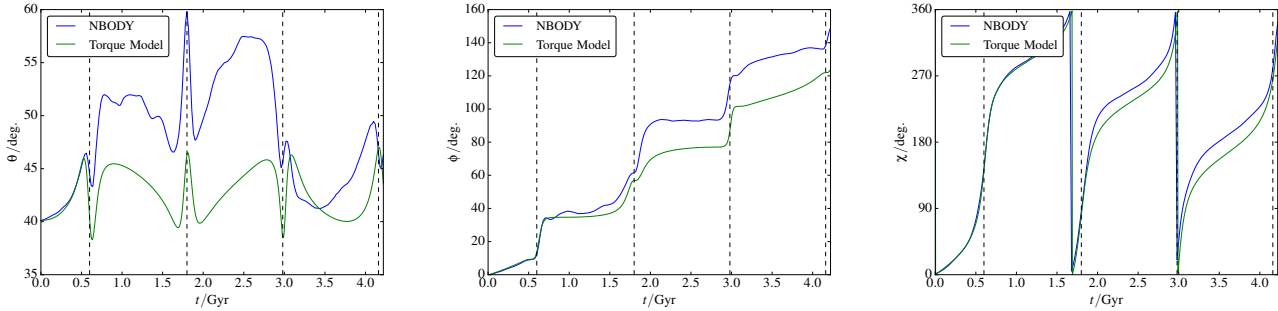


Figure 4. Evolution of the three orientation angles of the disk, as defined in Figure 3 in the simulation (blue) and as predicted from the formalism presented in section 3 (green). The times of the pericentre passages are indicated with dashed black lines. The NBODY and torque models agree closely until the first pericentre passage, after which the agreement is less exact. However there is good qualitative agreement over the entire period simulated.

is the angle between the projection of \mathbf{J}_{sat} onto the plane of the orbit and the Galactocentric x direction; finally, χ is the angle between the radial vector r and the projection of \mathbf{J}_{sat} onto the plane of the orbit. Figure 4 shows the evolution of each of the three angles defined above. The model specified by Equation 6 (green curve) can be compared with the actual trajectory of the disk’s pole (blue curve), as measured from the particles in the N-body simulation. The left panel of the Figure reveals a noticeable change in the misalignment angle between the disk and the orbital plane θ as a function of time. Fast dramatic oscillations in θ are visible around the times of the pericentre crossing. As the progenitor approaches the pericentre, the Galaxy pulls the disk’s nearest edge. Once passed, the other side of the disk is tugged, making it rock back and forth. Specifically, the sign of $d\theta/dt$ switches every time the disk’s viewing angle, χ , crosses an integer multiple of 90° , as illustrated in the right panel of Figure 4. The growth rate of χ is primarily governed by the orbital angular velocity of the progenitor and therefore depends on the eccentricity of the orbit. The orbit of the Sgr dwarf is rather eccentric and thus, around each pericentre, χ sweeps through more than 90° in a small fraction of the orbital period, causing fast oscillations in θ . On top of the periodic wobble seen in the left panel of the Figure, the Galaxy’s torques naturally also cause the disk to precess. This precession, i.e. the evolution of the angle ϕ , is shown in the middle panel of the Figure. Note that ϕ always evolves in the same direction, and over the course of the disruption, the amplitude of its change is much larger than that of θ .

Therefore we conjecture that: a) the overall difference *between* debris plane poles of individual streamlets result from the precession of the disk, i.e. changes in ϕ ; b) *within* each individual streamlet, the debris pole changes are caused by the combination of disk wobble and disk precession, i.e. changes in both θ and ϕ .

There is a good level of agreement between the model and the simulation: the formalism described above clearly is able to capture the qualitative behaviour. However, the actual disk wobble appears to be following a more complex pattern. We ascribe these differences to the changes in the satellite’s moment of inertia tensor that are not captured by our simple analytical torque model. Above, I_i are assumed to be constant. Yet, as the disk is disrupted by the Galaxy’s tides, its shape undergoes a dramatic evolution, as illustrated in Figure 5. As can be gleaned from the Figure, the disk dwarf is becoming more spherical as it sheds stars. This is indicated by each of the I_i s becoming closer in value as time progresses. This is in agreement with the earlier work of Mayer et al. (2001) who invoked this phenomenon to explain the morphological transformation of dwarf galaxies.

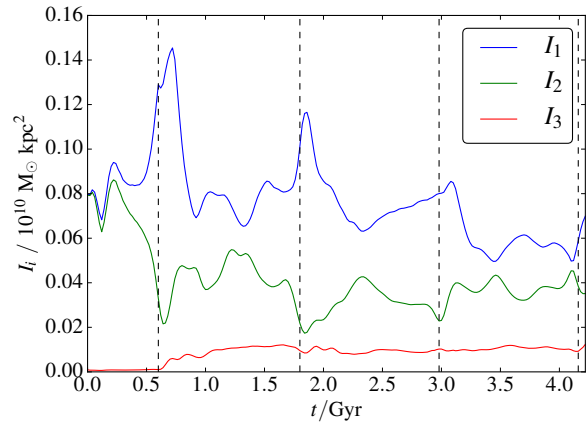


Figure 5. Evolution of the three principal axes of the moments of inertia tensor of the disk progenitor in the simulation with an initial misalignment angle of 40° . Note, that as material is being stripped, the disk is also stirred into a more spherical shape.

4 DISCUSSION AND CONCLUSIONS

It is natural to assume that the progenitor of the Sgr stream was most likely rotating. The luminous matter in the Sgr dwarf was reckoned by Niederste-Ostholt et al. (2012) to be $\sim 10^8 L_\odot$. This is the typical luminosity of dwarf irregular or dwarf elliptical galaxies, both of which possess intrinsic rotation. Therefore, the effects of rotation in the progenitor are probably important in understanding the properties of the Sgr tidal debris. Against this must be set the fact that the present day Sgr remnant is barely rotating at all (Peñarrubia et al. 2011; Frinchaboy et al. 2012).

It has long been hoped that precession of the debris plane, as inferred from the analysis of stellar streams like Sgr, can yield measurements of the flattening of the gravitational potential of the Milky Way. Orbits in a spherical potential are confined to a plane. Once the potential is made aspherical, then the plane begins to precess with a rate that depends on the flattening of the potential. However, as we have shown here, even in a spherical potential, the debris plane of a stellar stream might appear strongly to be “precessing” if it is produced by the disruption of a progenitor with a rotating disk, whose rotation is misaligned with the orbital plane.

We have established that the evolution of the debris plane along the stream (and along the individual streamlets, or branches) can also be caused by the disk wobbling and precessing during

the pericentre crossing. We have developed a simple model of the disk orientation and the corresponding stream “precession”, which captures the qualitative behaviour. Through tidal stirring, the progenitor’s moment of inertia tensor evolves away from its original configuration and so our simple model breaks down at large times. Thus, it is not yet possible to extend the fast and accurate stream models, similar to those discussed in Gibbons et al. (2014), to include rotating progenitors. Nevertheless, we find an encouraging level of agreement in the debris plane behaviour between our simulation and the Sgr stream measurements presented by Belokurov et al. (2014). We conclude that it is premature to discard the disk dwarf hypothesis of Peñarrubia et al. (2010) and caution against direct interpretation of the stream plane precession as caused by a non-spherical DM halo.

ACKNOWLEDGEMENTS

The authors thank the anonymous referee for a constructive report. SG thanks Michael Alexander for a thorough proofreading of the manuscript and acknowledges the Science and Technology Facilities Council (STFC) for the award of a studentship. The research leading to these results has received funding from the European Research Council under the European Union’s Seventh Framework Programme (FP/2007-2013) / ERC Grant Agreement no. 308024.

REFERENCES

- Abadi M. G., Navarro J. F., Fardal M., Babul A., Steinmetz M., 2010, *MNRAS*, 407, 435
- Allgood B., Flores R. A., Primack J. R., Kravtsov A. V., Wechsler R. H., Faltenbacher A., Bullock J. S., 2006, *MNRAS*, 367, 1781
- Amorisco N. C., 2015, *MNRAS*, 450, 575
- Amorisco N. C., Martínez-Delgado D., Schedler J., 2015, *ArXiv e-prints*
- Belokurov V., Koposov S. E., Evans N. W., Peñarrubia J., Irwin M. J., Smith M. C., Lewis G. F., Gieles M., Wilkinson M. I., Gilmore G., Olszewski E. W., Niederste-Ostholt M., 2014, *MNRAS*, 437, 116
- Belokurov V., Zucker D. B., Evans N. W. e. a., 2006, *ApJ*, 642, L137
- Boily C. M., Kroupa P., Peñarrubia-Garrido J., 2001, *New A*, 6, 27
- Bowden A., Belokurov V., Evans N. W., 2015, *MNRAS*, 449, 1391
- Davé R., Spergel D. N., Steinhardt P. J., Wandelt B. D., 2001, *ApJ*, 547, 574
- Debattista V. P., Moore B., Quinn T., Kazantzidis S., Maas R., Mayer L., Read J., Stadel J., 2008, *ApJ*, 681, 1076
- Dubinski J., Carlberg R. G., 1991, *ApJ*, 378, 496
- Fellhauer M., Belokurov V., Evans N. W., 2006, *ApJ*, 651, 167
- Frinchaboy P. M., Majewski S. R., Muñoz R. R., Law D. R., Łokas E. L., Kunkel W. E., Patterson R. J., Johnston K. V., 2012, *ApJ*, 756, 74
- Gibbons S. L. J., Belokurov V., Evans N. W., 2014, *MNRAS*, 445, 3788
- Gnedin O. Y., Gould A., Miralda-Escudé J., Zentner A. R., 2005, *ApJ*, 634, 344
- Hayashi E., Navarro J. F., Springel V., 2007, *MNRAS*, 377, 50
- Helmi A., 2004, *ApJ*, 610, L97
- Johnston K. V., Law D. R., Majewski S. R., 2005, *ApJ*, 619, 800
- Kazantzidis S., Kravtsov A. V., Zentner A. R., Allgood B., Nagai D., Moore B., 2004, *ApJ*, 611, L73
- Koposov S. E., Belokurov V., Evans N. W., et. al. 2012, *ApJ*, 750, 80
- Koposov S. E., Rix H.-W., Hogg D. W., 2010, *ApJ*, 712, 260
- Küpper A. H. W., Balbinot E., Bonaca A., Johnston K. V., Hogg D. W., Kroupa P., Santiago B. X., 2015, *ApJ*, 803, 80
- Law D. R., Johnston K. V., Majewski S. R., 2005, *ApJ*, 619, 807
- Law D. R., Majewski S. R., 2010, *ApJ*, 714, 229
- Leaman R., Venn K. A., Brooks A. M., Battaglia G., Cole A. A., Ibata R. A., Irwin M. J., McConnachie A. W., Mendel J. T., Tolstoy E., 2012, *ApJ*, 750, 33
- Loebman S. R., Ivezić Ž., Quinn T. R., Governato F., Brooks A. M., Christensen C. R., Jurić M., 2012, *ApJ*, 758, L23
- Macciò A. V., Dutton A. A., van den Bosch F. C., 2008, *MNRAS*, 391, 1940
- Mayer L., Governato F., Colpi M., Moore B., Quinn T., Wadsley J., Stadel J., Lake G., 2001, *ApJ*, 559, 754
- Mayer L., Moore B., Quinn T., Governato F., Stadel J., 2002, *MNRAS*, 336, 119
- Navarro J. F., Frenk C. S., White S. D. M., 1996, *ApJ*, 462, 563
- Niederste-Ostholt M., Belokurov V., Evans N. W., 2012, *MNRAS*, 422, 207
- Niederste-Ostholt M., Belokurov V., Evans N. W., Peñarrubia J., 2010, *ApJ*, 712, 516
- Peñarrubia J., Belokurov V., Evans N. W., Martínez-Delgado D., Gilmore G., Irwin M., Niederste-Ostholt M., Zucker D. B., 2010, *MNRAS*, 408, L26
- Peñarrubia J., Zucker D. B., Irwin M. J., Hyde E. A., Lane R. R., Lewis G. F., Gilmore G., Wyn Evans N., Belokurov V., 2011, *ApJ*, 727, L2
- Smith M. C., Evans N. W., An J. H., 2009, *ApJ*, 698, 1110
- Springel V., 2005, *MNRAS*, 364, 1105
- Vera-Ciro C. A., Sales L. V., Helmi A., Frenk C. S., Navarro J. F., Springel V., Vogelsberger M., White S. D. M., 2011, *MNRAS*, 416, 1377
- Yu Q., Madau P., 2007, *MNRAS*, 379, 1293